AN ATTEMPT TO MODEL STORM-TIME CHANGES IN UPPER THERMOSPHERIC MASS DENSITY WITH NRLMSISE-00 AND CHAMP AIR DRAG DATA

Ma S. Y. [(1)], Luehr H. [(2)], Zhou Y. L. [(1,2)], Cai L. [(1)], Dang G. [(1)], Wang H. [(1,2)] and Reigber C. [(2)]

[(1)] Inst. of Ionosphere and Magnetosphere, LOGEG, CNME;
College of Electronic Informatics, Wuhan University, Wuhan 430079, P. R. China;
[(2)] GeoForschungsZentrum Potsdam, 14473, Germany

ABSTRACT

A study is made on the global changes of air mass density in upper thermosphere during major magnetic storms by using accelerometer measurements on board CHAMP, taking NRLMSISE-00 model-predicted densities as a reference. More than 20 storm events in 2001-2004 are used to make a comprehensive statistics. The dependences of the storm-time changes in mass density on both the global Joule heating power and Sym-H index are investigated. An empirical relation connecting mass density changes around 400 km height with the two control parameters is worked out for different latitude and sunlight. Adding a correction calculated from the empirical relation to the NRLMSISE-00 model reference leads to a much better prediction of storm-time thermospheric mass density.

1. INTRODUCTION

The spatial distribution of the thermospheric mass density would change greatly during magnetic storms due to largely enhanced Joule heating forcing [1, 2] at high latitudes and other possible sources of neutral particles and heating associated with dynamic processes in the ring currents [3]. The heating drive airs upwelling in the source region and circulating globally, causing strong disturbances of the composition and hence the total mass density in the thermosphere on a height surface, especially in the ionospheric F region where the mass density increase remarkably. On the other hand, there may also occur local low-density holes and wave-like structures [4]. These cause an increase or fluctuate of air drag on the flying satellite, being the dominant sources of error in orbital tracking/prediction of spacecraft below 1000 km altitude.

Study on the global distribution of storm-time changes in the thermospheric mass density is of great importance for improving the current thermospheric model aiming to space weather forecast. Sensitive tri-axial accelerometer on board of Germany CHAMP satellite provides new and high-quality data of air drag for low-orbiting spacecraft. Some issues newly published [5-7] show a large deviation of atmospheric mass density observed by CHAMP from that predicted by models such as MSISE-90, NRLMSISE-00 etc. during great magnetic storms.

The present work studies the global distribution of total mass density changes at about 400 km height versus latitude and sunlight during major magnetic storms by using STAR accelerometer measurements on board CHAMP, focusing on their dependence of Joule heating and ring current index in order to improve the current thermospheric model aiming to space weather forecast.

2. DATA AND PROCESSING

2.1 Derivation of Mass Density

The atmospheric mass densities are derived from air drag measured by CHAMP STAR accelerometer according to the following equation [8, 9]:

$$\vec{a}_{drag} = -\frac{1}{2}\rho\frac{C_d}{m}Av^2\frac{\vec{v}}{v}$$

$$\Rightarrow \qquad \rho = -\frac{2a_{drag}m}{C_d A v^2} \qquad (1)$$

where a_{drag} is the acceleration caused by air drag, ρ is the atmospheric total mass density, C_d is the drag coefficient, A is the effective cross-sectional area of satellite in the ram direction, m is the satellite mass, v is the relative velocity of the satellite to the atmosphere. All density are normalized to 400 km by

$$\rho_{400} = \rho_h e^{\frac{h-400}{H}} \qquad (2)$$

where ρ_{400} is the normalized density at 400 km, ρ_h is the density at orbit height h, H is the scale height calculated by NRLMSISE-00 [10].

2.2 Calculation of Storm-Time Changes in Mass Density

Taking the mass density computed from NRLMSISE -00 without active Ap index input as a reference, the storm-time changes are calculated as the deviations of CHAMP derived mass density from the reference.

2.3 Selection of Storms

Total 20 magnetic storm events are used in present study. All they have Min. Dst less than -100 nT as listed in table 1. During these storms solar wind and IMF data from ACE spacecraft are available to calculate Joule heating.

Table 1. List of the selected 20 storm events

Date	Min. Dst (nT)	Date	Min. Dst (nT)
Sep. 25-26, 2001	-102	Nov. 20-21, 2002	-128
Oct. 01-05, 2001	-166	May 29-31, 2003	-131
Oct. 21-24, 2001	-187	Aug. 17-19, 2003	-168
Nov. 05-06, 2001	-292	Oct. 29-31, 2003	-401
Mar. 23-25, 2002	-100	Nov. 20-21, 2003	-472
Apr. 17-21, 2002	-149	Jan. 22-27, 2004	-149
May 23-25, 2002	-109	Feb. 11-12, 2004	-109
Aug. 20-21, 2002	-106	Apr. 03-04, 2004	-112
Sep. 07-09, 2002	-181	Jul. 24-30, 2004	-197
Oct. 01-03, 2002	-176	Aug. 30-31, 2004	-126

2.4 Calculation of Joule Heating

Height-integrated Joule heating Q_J as a function of geomagnetic latitude and MLT is estimated as

$$Q_J = \Sigma_p E_\perp^2 \qquad (3)$$

where, $\sum_p$ is height-integrated Pedersen conductivity, $E_\perp$ is convection electrical field. We use Wiemer potential model [11] to calculate convection electrical field. Conductivity component caused by particle precipitation follows empirical relation as[12]：

$$\Sigma_{p,p} = \frac{40E_0}{16+E_0^2}\sqrt{I} \qquad (4)$$

where E_0 is the average energy of precipitation electrons, I is the integrated energy flux(in erg/cm^{2}s). E_0 and I are obtained from an empirical model of auroral electron precipitation developed by wuhan university group based on EISCAT/FAST data (private communication). Solar radiation conductivity is calculated using relation [13]:

$$\Sigma_{p,s} = 0.88(S_\alpha \cos\chi)^{0.5} \qquad (5)$$

The total Pedersen conductivity is obtained by

$$\Sigma_p = \sqrt{\Sigma_{p,s}^2 + \Sigma_{p,p}^2} \qquad (6)$$

The total Joule heating power, $\sum Q_J$, is an integration of Q_J over latitude and MLT:

$$\Sigma Q_J = \iint Q_J(\theta,\varphi)\mathrm{d}\theta\mathrm{d}\varphi \qquad (7)$$

The high-resolution ring current index of Sym-H are from WDC-2 (http://swdcdb.kugi.kyoto-u.ac.jp).

Figure 1 gives an example of storm-time variation of mass density as seen by CHAMP and predicted by NRLMSISE-00, ring current index of Sym-H, total Joule heating power, as well as location latitude of the maximum of Joule heating for the November 2003 storm.

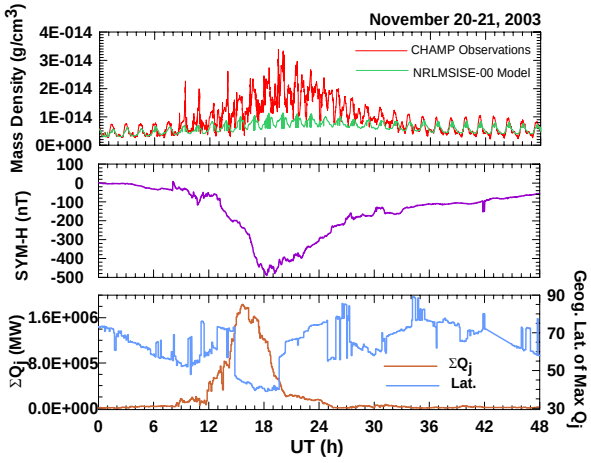

Figure 1. Temporal variation of mass density by both CHAMP and NRLMSISE-00 model(top), Sym-H index (middle), total Joule heating power and the location latitude of the maximum Joule heating (bottom).

We collected such plots and corresponding digital data for all the selected 20 storms.

3. METHOD OF MODELING

3.1 Grid in the Frame of Latitude and LT

In order to find the dependences of the storm-time mass density changes on the $\sum Q_J$ and Sym-H for different latitude and sunlight, we sort the density changes into 70 grids of latitude by LT. The geographic latitude ranging from 85˚S to 85˚N is divided into 35 groups with an interval of 5º. Due to limitation of storm-time data, the local time is divided only two groups, i. e., the day-side and the dark-side. Thus there are 70 grids globally. For each orbit, the storm-time changes are averaged over every grid, so that we can get a time (orbit) sequence of mass density changes at a certain grid for each storm. Figure 2a shows some examples of time (orbit) sequences of storm-time changes in mass density on the dark-side at different latitude for November 2003 storm. Figure 2b gives the same ones as figure 2 but for day-side.

Comparison with Sym-H and total Joule heating as shown in figure 1, it seems that the variations of mass density changes at different latitudes are dependent strongly on these two parameters. Below we will examine this dependence in detail.

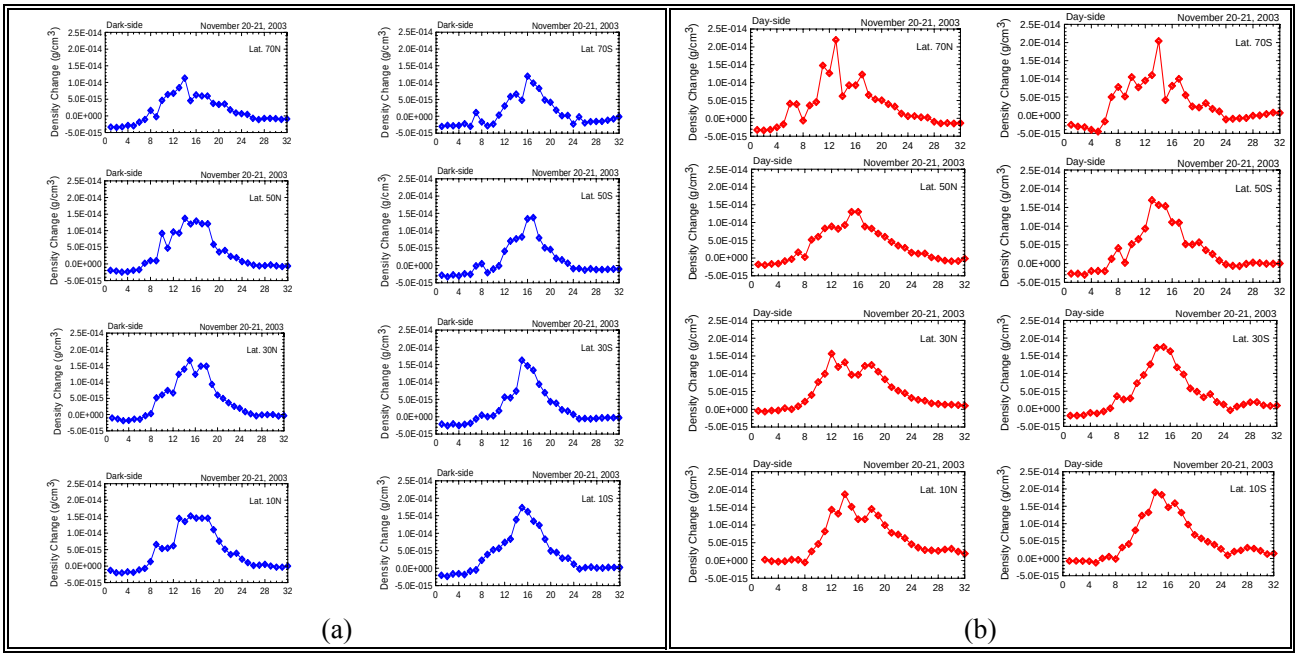

Figure 2. Time (orbit) sequences of storm-time mass density changes at different latitudes on the dark-side (left panel a) and the day-side (right panel b) for the storm of November, 2003.

3.2 Cross-Correlation

By calculating cross-correlation, the lag times of mass density changes behind Sym-H and $\sum Q_J$ are obtained for each storm and each grid, along with the maximum correlation coefficients. Figure 3 shows an example of the lag times and correlation coefficients for the storm of November 2003.

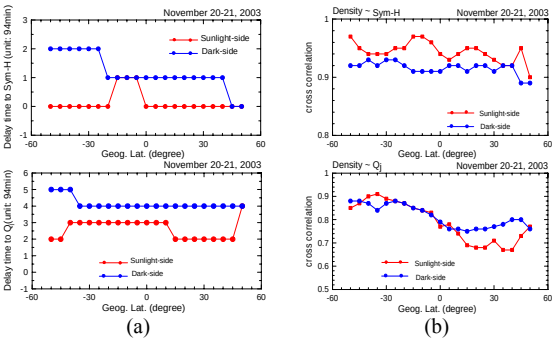

Figure 3. (a) The lag times of mass density changes behind Sym-H (top) and $\sum Q_J$ (bottomt) for dayside (red) and dark-side (blue) at different latitudes during magnetic storm of November 2003; (b) The same as (a) but for linear correlation coefficients between mass density changes with Sym-H and $\sum Q_J$.

It shows that the changes in mass density are correlated closely with Joule heating and ring current index and it lagged behind the Joule heating by 3~7 hours and behind the Sym-H by 0~3 hours. The delay times are much longer at lower latitude on the dark-side. The delay is mainly related to the propagation of the density disturbance out from heat source region.

Figure 4 gives spot plots of mass density changes versus the Sym-H index and the total Joule heating for November 2003 storm, where the latter two parameters have been shifted by a certain time upon the lag times estimated above. It is seen that mass density changes are proportional to the shifted Sym-H index and total Joule heating.

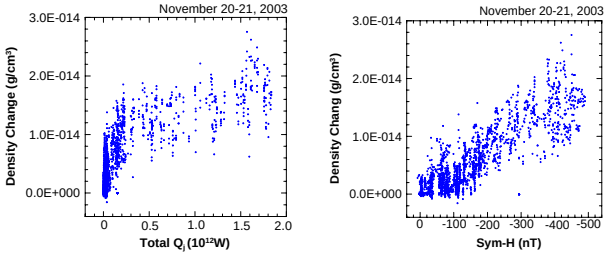

Figure 4. Spot plots of mass density changes versus $\sum Q_J$ (left) and Sym-H (right) for November 2003 storm. The time sequence of $\sum Q_J$ and Sym-H have been shifted upon the lag times.

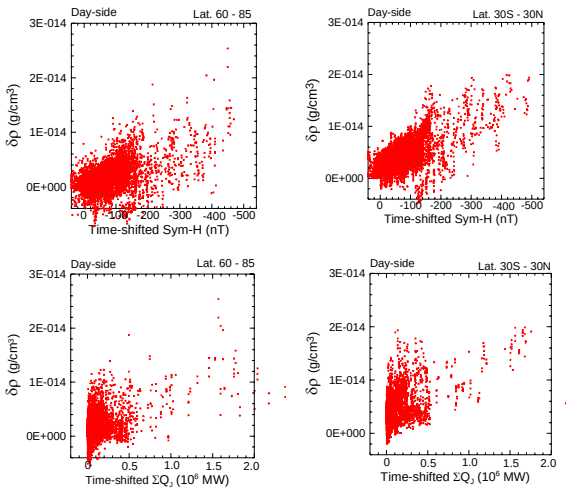

Figure 5. The same as figure 4, but for all the 20 storms on day-side at higher latitudes (left) and lower latitudes (right).

Figure 5 shows the spot plots of mass density changes versus Sym-H index and total Joule heating for all the 20 selected storms at two different latitude zones centered at the equator and the auroral region respectively.

As a whole, these spot plots show nearly linear relations of storm-time changes in thermospheric mass density with the two parameters.

3.3 Multiple Linear Regression

By using multiple linear regression with proper time shift, an empirical relation of storm-time mass density changes at about 400km versus Sym-H index and total Joule heating is worked out for every grid of MLat×MLT as following:

$$\delta\rho = P_0 + P_1 \cdot SymH + P_2 \cdot \sum Q_j \qquad (7)$$

where δρ is changes in thermospheric mass density, P_0, P_1 and P_2 are the fit coefficients.

Figure 6 shows the fit coefficients of multiple linear regression versus latitude for different sunlight.

It is seen that the regression coefficients for Joule heating term has a lager weight at middle-high latitudes, while that for Sym-H index larger at low-latitudes, being reasonably consistent with physics. These coefficients provide an empirical relation connecting storm-time changes in mass density around 400 km height with Sym-H and $\sum Q_J$ at different latitudes and sunlight.

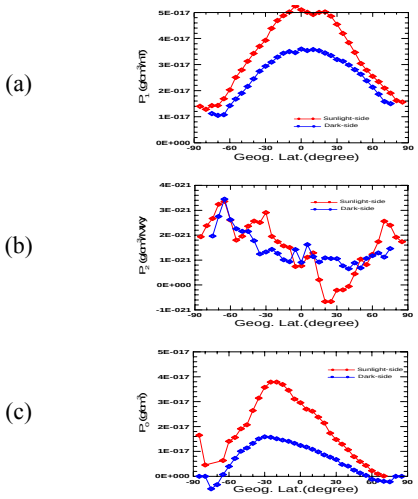

Figure 6. Fit coefficients of multiple linear regression. (a) Coefficient P_1 for Sym-H term; (b) Coefficient P_2 for $\sum Q_J$ term; (c) Coefficient of intercept, P_0.

4. APPLICATION

The empirical relation established above may serve as a correction to the NRLMSIS-00 model. Adding the storm-time changes in mass density calculated by the empirical relation to the reference density modeled by NRLMSISE-00 with only daily Ap index input results in a corrected density. Figure 7 gives an example of applying the empirical relation to the storm occurring on July 16, 2003.

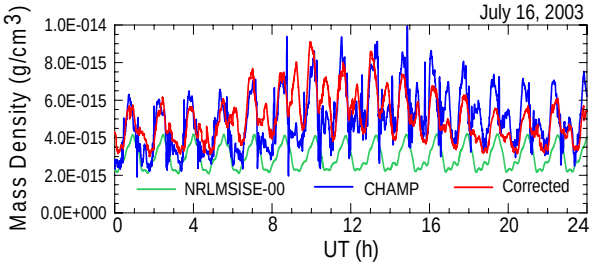

Figure 7. Comparison of the mass density observed by CHAMP (blue), modeled by NRLMSISE-00 (green) and the corrected density (red) on July 16, 2003, where the corrected density is the sum of the density predicted by NRLMSIS-00 model taking daily Ap as input and that calculated by the empirical relation.

It is seen clearly that the corrected mass density can reproduce the CHAMP observed storm-time mass density much better than that modeled by NRLMSISE -00. During 10:00-16:00 UT, the average deviation from the CHAMP observation is 0.2350×10^{-15} g/cm^3 for the corrected density, while 2.5874×10^{-15} g/cm^3 for NRLMSIS-00 modeled density.

5. CONCLUSION

The main results of this study are outlined as follows:

(1) The NRLMSISE-00 model is unable to describe well the enhancements in the thermospheric mass density observed by CHAMP at about 400km during great geomagnetic storms. CHAMP STAR accelero meter measurements provide valuable data sets to improve the model.

(2) By calculating the cross correlation function of the storm-time mass density changes versus the Sym-H index and the total Joule heating, it reveal that the mass density changes are correlated closely with these two parameters, having proper time-lags behind them.

(3) An empirical relation connecting the storm-time changes in mass density with Sym-H index and total Joule heating is worked out by multiple linear regression by using CHAMP-observed mass density data during 20 storms in 2001 to 2004.

(4) The empirical relation may serve as a correction to the NRLMSIS-00 model. It indicates that the correction term for Joule heating has a larger weight at middle-high latitudes, while that for Sym-H index larger at low-latitudes.

(5) Adding the correction calculated by the empirical relation to the NRLMSISE-00 model leads to a much better prediction of storm-time thermospheric mass density at about 400 km altitudes.

It is in prospect that the SWARM mission would provide much more useful air drag data measured in multiple points to improve the existing model further.

Acknowledgments. The operational and data processing supports of the CHAMP mission by DLR and BMBF are gratefully acknowledged. This study is supported by National Nature Science Foundation of China (No. 40390150).

References

1. Fuller-Rowell T. J. et al., *Magnetic storms, Geophysical Monograph Series*, Vol. 98, edit. Tsurutani B. T. et al., 203-225, AG U, 1997.
2. Proelss G. W., *Magnetic storms, Geoph- ysical Monograph Series*, Vol. 98, edit. Tsurutani B. T. et al., p 227-241, AGU, 1997.
3. Daglis L. A. et al., *Reviews of Geophysics*, Vol. 37, No. 4, 407-438, 1999.
4. Fuller-Rowell T. J. et al., *Advances in Space Research*, Vol. 24, Issue 11, 1447- 1458, 1999.
5. Liu, H., and H. Lühr, *J. Geophys. Res.*, *110*, A09S29, doi:10.1029/2004JA010908, 2005.
6. Forbes, J. M. et al., *J. Geophys. Res*., 101, A12S27, doi:10.1029/2004JA010856,2005.
7. Sutton E. K., J. M. Forbes, and R. S. Nerem, *J. Geophys. Res*., 110, A09S40, doi:10.1029/2004 JA010985, 2005.
8. Lühr H. et al., *Geophys. Res. Lett.*, Vol. 31, L06805, doi:10.1029/2003GL019314, 2004.
9. Bruinsma, S., D. Tamagnan, and R. Biancale, *Planet. Space Sci.*, Vol. 52, 297– 312, 2004.
10. Picone J. M. et al., *J. Geophys. Res.*, Vol. 107, No. A12, 1468, doi:10.1029/2002 JA009430, 2002.
11. Weimer, D. R, *J. Geophys. Res.*, Vol. 106, A1, 407-416, 2001.
12. Robinson, R. M. and Vondrak R. R., *J. Geophys. Res.*, Vol. 89, No.A6, 3951-3956, 1984.
13. Robinson R. M., Vondrak R. R., Friis- Christensen E., *Geophys. Res. Letters*, Vol. 14, 656-659, 1987.